

# Alternation of the Mode Synchronization and Desynchronization in Ultrafast Fiber Laser

Yueqing Du, Sergey V. Sergeyev, Zuowei Xu, Mengmeng Han, Xuewen Shu,\*  
and Sergei K. Turitsyn

Ultrafast fiber lasers offer a unique opportunity to implement optically a Poincaré mapping in the phase space of a variety of complex dissipative dynamical systems operating far from the equilibrium. Understanding of such complex optical dynamical systems revealing, for instance, ultrafast dynamics of the dissipative solitons (DSs) and more complex regimes is important for advancing specification and performance of the mode-locked lasers used in a vast number of applications ranging from spectroscopy and medicine to metrology and telecom. Here, using the mode-locked fiber laser as a test-bed, the Shilnikov-type ultrafast dynamics taking the form of randomly switching between noise-like pulsing and quasi-continuous-wave regimes is experimentally demonstrated. The transient coherence recovery is revealed, during which the noise-like pulse (NLP) is transformed into a coherent DS state and then returned to an incoherent NLP state. The demonstrated alternation of mode synchronization and desynchronization is both of practical importance for developing new types of partially mode-locked lasers and of the fundamental interest for the nonlinear science in the context of revealing routes to the turbulence in distributed nonlinear systems.

nonlinearity, gain, and loss.<sup>[4,5]</sup> Coherent pulses with high quality mode-locking known as dissipative solitons present a simple variant of a balance between key physical cavity effects. In addition to the coherent DS, various partially coherent and incoherent spatiotemporal structures can exist in the dissipative systems,<sup>[6–16]</sup> which can be regarded as the chaotic attractors of the dissipative systems<sup>[17]</sup> and transformed by tuning the parameters of the laser system.<sup>[18–25]</sup> Laser systems are naturally described by the mathematical Poincaré mapping in the phase space of the key field parameters. Therefore, lasers present both important practical devices and interesting physical systems with rich nonlinear dynamics. Revealing and understanding various types of the ultrafast dynamics in dissipative systems is a challenging fundamental problem with potential for numerous

## 1. Introduction

Mode-locked fiber lasers generating pulse trains with femtosecond scale pulse trains are essential tools for micromachining, fluorescence microscopy, frequency combs generation and the other applications.<sup>[1–3]</sup> The dynamics of ultrashort pulses in dissipative systems like mode-locked lasers and microresonators include interlacing complex physical effects such as dispersion,

applications ranging from secure communications to micromachining. The transformation of the attractors of the ultrafast system usually requires the manual adjustment of the parameters. However, the attractors can be changed without manual adjustment when there is an internal perturbation in the system. Tri-stable state in a passive fiber cavity can be obtained when the light is perturbed by the stimulated-Raman-scattering.<sup>[26]</sup> Also in the passive fiber cavity,<sup>[27]</sup> it has been theoretically shown that the solution starting from a perturbed saddle point can move toward two attractors. The DS in a fiber laser perturbed by a dual-hump filter can periodically switch between two states.<sup>[28]</sup> The self-transformation of the ultrafast states in dissipative systems is significant for understanding the ultimate limitation on the mode-locking and the frequency comb stabilization in ultrafast light sources.

When the ultrafast laser operates in the highly nonlinear regime, the pulse train will deviate from the stationary state, accompanying with the loss of shot-to-shot coherence, which is termed as the partially mode-locked states in the literature.<sup>[10]</sup> The stochastic and transient dynamics of the partially mode-locked states are of great interest because of their limitation on the stability of the ultrafast fiber laser and their potential for secure communications. A nonlinear-polarization-rotation (NPR) fiber laser exhibits internal perturbations on ultrafast pulses due to an effective non-monotonic saturable absorber.<sup>[29,30]</sup> It is easy to

Y. Du, Z. Xu, Dr. M. Han, Prof. X. Shu  
Wuhan National Laboratory for Optoelectronics and School of Optical  
and Electronic Information  
Huazhong University of Science and Technology  
Wuhan 430074, China  
E-mail: xshu@hust.edu.cn

Dr. S. V. Sergeyev, Prof. S. K. Turitsyn  
Aston Institute of Photonics Technologies  
Aston University  
Birmingham B4 7ET, UK

Prof. S. K. Turitsyn  
Aston-NSU Centre for Photonics  
Novosibirsk State University  
Novosibirsk 630090, Russia

 The ORCID identification number(s) for the author(s) of this article can be found under <https://doi.org/10.1002/lpor.201900219>

DOI: 10.1002/lpor.201900219

adjust the NPR laser to a stochastically or partially mode-locked state with strong alternation of its lasing states, which is usually avoided aiming at stability. Mode-desynchronization in the laser cavity generates quasi-continuous waves (quasi-CW) while mode synchronization produces stable mode-locking short-pulse trains. By tuning the polarization controller (PC) of the NPR laser, we found the laser can continuously alternate between the mode synchronization and desynchronization. Moreover, the spectrum of this lasing state measured by the optical spectrum analyzer (OSA) shows clear composite characteristics of the DS, NLP, and quasi-CW. We call this specific partially mode-locked state a composite mode-locked (CML) behavior.

The dispersive-Fourier transform (DFT)<sup>[31]</sup> is a powerful tool that has been used to study the dynamics of ultrafast lasers<sup>[10,14,16,32–36]</sup> in recent years. The dynamics and mechanism of the observed CML are revealed by using the DFT technique. The quasi-CW, coherent DS, and incoherent noise-like pulse (NLP) coexist in the laser without strong external perturbations. The transient coherence recovery is observed during the CML, during which the incoherent NLP pulse transforms into a coherent DS for an instant, and then recovers to the NLP. The peak power and energy enhancement of the pulse during the transient coherence recovery result in the adjustment of the parameters

of the artificial SA and the slow dynamics of the gain fiber,<sup>[37,38]</sup> which led to a transformation of the lasing states. The results offer novel insights into the transient dynamics and better understanding of mode synchronization and desynchronization in ultrafast lasers.

## 2. Results

### 2.1. States Switching

In the CML state of the laser, the spectrum measured by the OSA is cut into pieces, as shown in **Figure 1a**; this looks like a broadband NLP spectrum together with a narrow peak. The dips in the **Figure 1a** mean that there was lasing state transformation during the OSA scanning. The spectrum in linear scale in **Figure 1a** has a strong narrowband peak, together with a weak and broadband pedestal, which is common during the adjustment of mode-locked lasers. The local enlargement of the pedestal in **Figure 1b** shows that the peak wavelength of the pedestal is  $\approx 1577$  nm, while the wavelength of the narrowband peak is  $\approx 1569$  nm. The intensity evolution of the DFT signals over 190 000 round trips (RTs) with a sampling rate of  $10 \text{ GS s}^{-1}$  was captured and shown in **Figure 1c**, where we can see the lasing state transformation.

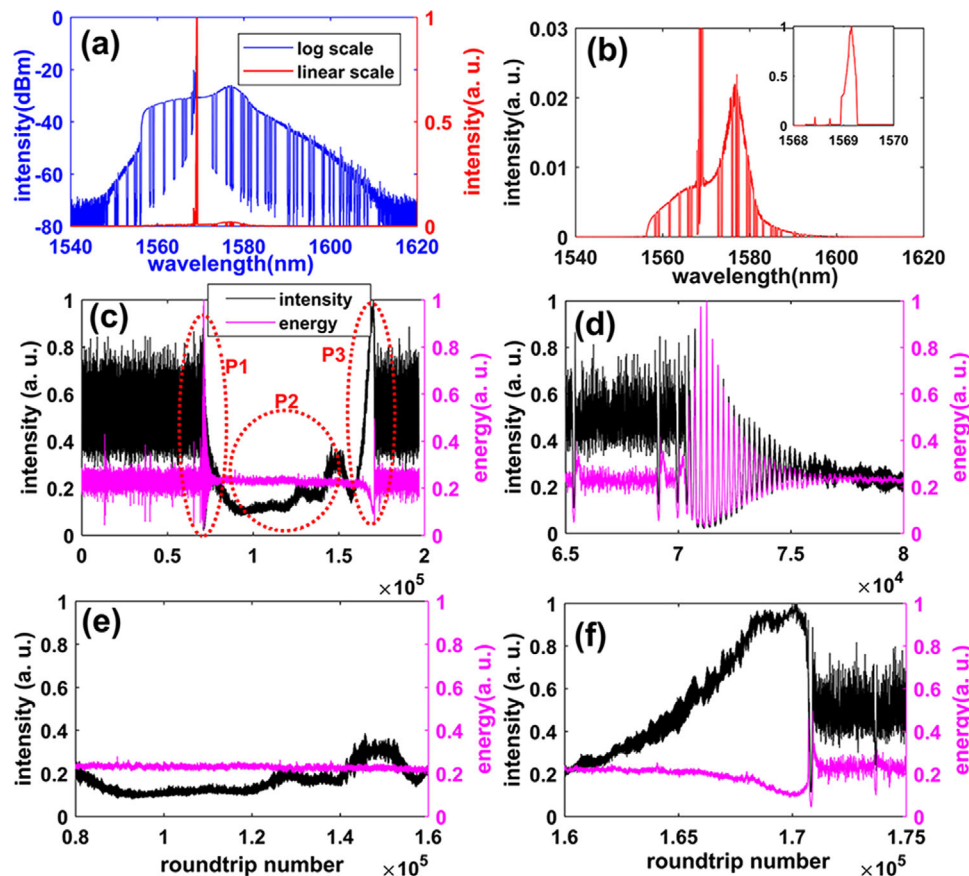


**Figure 1.** a) Spectrum of the laser output measured by the OSA in log (blue solid) and linear (red solid) scales. b) Local enlargement of the pedestal of the spectrum in linear scale. c) Intensity and energy evolution in 190 000 RTs. d) Local enlargement of the marked portion P1 in (c). e) Local enlargement of the marked portion P2 in (c). f) Local enlargement of the marked portion P3 in (c). The inset in (b) is the local enlargement of the narrow peak of the spectrum in linear scale. The sampling rate of the oscilloscope (OSC) for the stretched signal measurement in (c)–(f) is  $10 \text{ GS s}^{-1}$ .

For clarity, we mark three processes in Figure 1c with P1, P2, and P3, and their enlargement portions are shown in Figure 1d–f, respectively. Before P1, the power and energy evolve stochastically. The stochastic state transforms into a “quiet” state, with weak fluctuations in the intensity and energy after the decreased relaxation-oscillation (RO), as shown in Figure 1d. The energy of the wave in the “quiet” state keeps a relatively constant level, while the intensity gradually increases as we can see from Figure 1e. In Figure 1f, the lasing state transforms from the “quiet” state in P2 to the stochastic state through the transition process of P3. The intensity increases while the energy decreases from the 160 000th to 170 000th RTs. After the intensity and energy reach their maximum and minimum, respectively, the lasing state experiences a transient process and then transforms into a stochastic state again. We can see from Figure 1c–f that the spectrum measured by the OSA in Figure 1a was caused by the lasing state transformation. There are complex dynamics during the wave evolution in the CML state, which we will thoroughly characterize by the DFT in the subsequent sections.

## 2.2. From Quasi-CW to NLP

To characterize the evolution dynamics of the state in Figure 1, several key processes of the DFT signals are captured with the

laser parameters kept fixed. The process similar to P3 in Figure 1 is shown in **Figure 2**. A clear lasing state transformation from the “quiet” state to the stochastic state in the 40 000 captured RTs is shown in Figure 2a. The local enlargement of the state transition marked in Figure 2a is shown in Figure 2b for clarity. Five points in Figure 2b are marked with A–E, respectively. The intensity and energy of the DFT signals experienced dramatic evolution from A to E. Figure 2c is the spatio-spectral evolution corresponding to Figure 2a, where we can see clear alternation from the mode desynchronization to synchronization. We should emphasize that the periodic NLP train emitted from the laser should be treated not as a traditional mode-locked regime, but rather as a partially mode-locked state that keep features the pulse localization and periodic property in the temporal domain. However, the NLP loses the shot-to-shot coherence due to the strong nonlinearity and corresponding instabilities and nonlinear interactions.<sup>[10]</sup> A narrowband pulse builds up from the quasi-CW from the 1st to 26 000th RTs and then evolved into the incoherent NLP state with strong spectral broadening, which is shown in Figure 2c. Thus, the “quiet” and stochastic lasing states in Figures 1 and 2 are the quasi-CW and NLP, respectively. The NLP is confirmed by the stochastic fluctuations and the fine structures in the spatio-spectral evolution.<sup>[12]</sup> The local enlargement of the marked portion in Figure 2c is plotted in Figure 2d. From A to B in

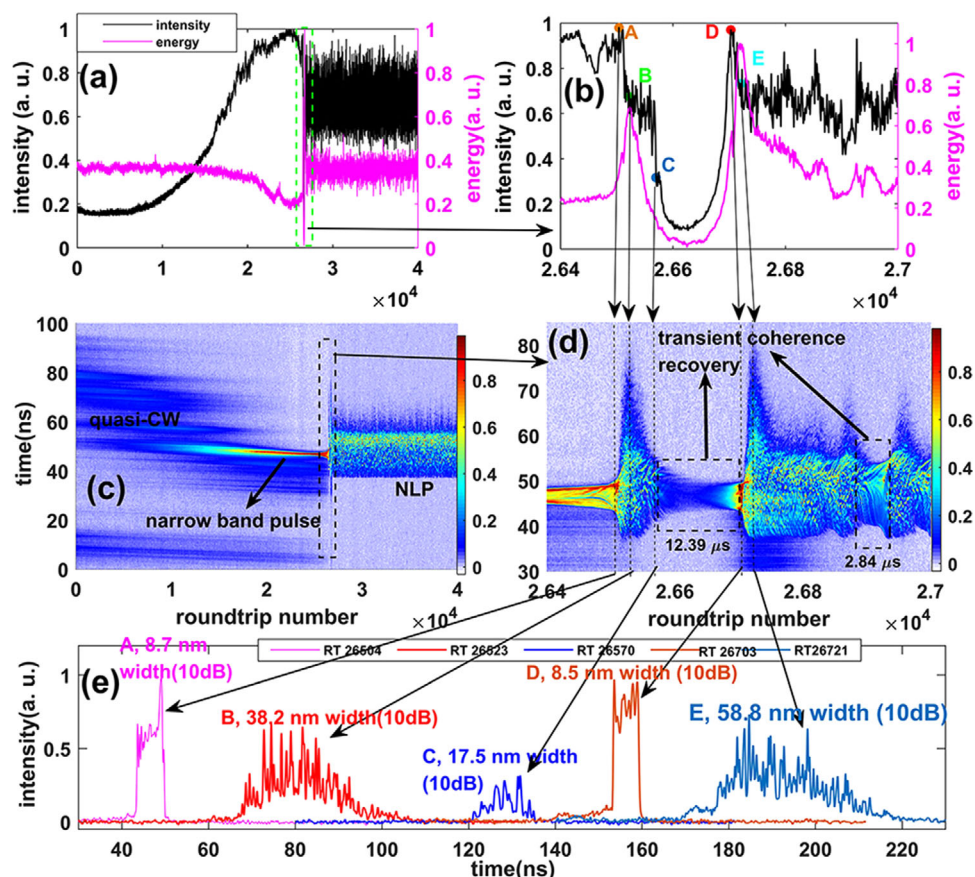


**Figure 2.** Dynamics of the stretched signals for laser transition from the quasi-CW to the NLP state. The sampling rate of the OSC is  $20 \text{ GS}^{-1}$ . a) Intensity and energy evolution in 40 000 RTs. b) Local enlargement of the marked portion in Figure 2a. c) Stretched signal evolution of the 40 000 RTs. d) Stretched signal evolution from the 26 000th to 27 000th RTs. e) Five single-shot DFT signals at the 26 044th, 26 523rd, 26 570th, 26 703rd, and 26 721st RTs.

Figure 2d, the spectrum of the pulse transforms from a coherent state into an incoherent state with stochastic structures. The spectrum gradually evolves to a coherent state with a narrowband spectrum from B to C. The coherent state sustains from C to D for  $\approx 130$  RTs and reaches the maximum intensity at D. The energy and spectral width experiences dramatic increasing and then reaches an incoherent NLP state from D to E. The pulse at D has maximum intensity while E has maximum energy, which correspond to the coherent DS and incoherent NLP, respectively. Besides the transient coherence recovery from C to D, there is another transient coherence recovery process at the  $\approx 26\,890$ th RT, which is marked in Figure 2d. The durations of the 1st and 2nd coherence recovery processes in Figure 2d are 12.39 and 2.84  $\mu\text{s}$ , respectively. The higher the energy of the DS, the shorter duration of the coherence recovery. This is because the peak power of the DS is roughly proportional to the pulse energy and the higher peak power contribute to the larger nonlinear phase accumulation of the DS and shift the feedback region of the NPR modelocker, thus making the duration of the DS shorter. The single-shot spectra of A–E are shown in Figure 2e. The spectra of A and D have typical steep edges while the spectra of B and E have broadband spectra with stochastic structures. Point C is an intermediate state between the coherent DS and incoherent NLP. The transient coherence recovery during B–E sustains for  $\approx 199$  RTs ( $\approx 0.202$  ms), which is very short-lived compared to the build-up from the quasi-CW to NLP with a duration of  $\approx 27.3$  ms. We can see from Figure 2 that the DS is unstable and quickly evolves into the NLP, which can be regarded as the saddle solution for the laser.

The qualitative explanation of the transition in Figure 2 can be described as follows: the coherent DS at A collapses into the incoherent NLP at B due to the over-driving of the NPR as well as the strong nonlinearity for the coherent DS with strong peak power. The gain of the Erbium-doped fiber (EDF) is saturated by the enhanced pulse at B, the NPR effect together with the saturated gain gradually drive the NLP into the coherent DS state. Due to the strong energy decreasing after C, the coherent DS experienced strong amplification until it reaches its maximum at D, resulting in the over-driving of the NPR again. The coherent DS collapses into the incoherent NLP at E and then keeps the NLP evolution. There is another transient coherence recovery with shorter duration and broader spectrum than the first one after the 26 800th RT. In a word, the results in Figure 2 characterize the process in which a narrowband pulse emerged from the quasi-CW state and finally evolved into the NLP. Visualization S1, Supporting Information, offers the vivid dynamics in Figure 2d.

### 2.3. Transient Coherence Recovery During the NLP

With the mode-locking state kept fixed as in Figure 2, the transient coherence recovery also happens during the NLP evolution, as shown in Figure 3. We can see from Figure 3a that the NLP evolution was occasionally disrupted, manifesting as many tips and dips. The embedded intervals in the spatio-spectral evolution in Figure 3b correspond to the tips and dips in Figure 3a. The enlargement visualization of the marked portion and its related

spatio-spectral evolution in Figure 3a are shown in Figures 3c and 3d, respectively. The intensity of the stretched pulse in the dips in Figure 3c has weak fluctuations. The two dips in Figure 3c has durations of 159 and 176 RTs, respectively. The evolution in Figure 3d demonstrates the dips in Figures 3a,c corresponding to the transient coherence recovery. The complicated fringes in the spectrum of the NLP in Figure 3d are gradually focused to a small region and then swept out of the spectrum, which is caused by the transformation of the temporal chirp of the pulse from the nonlinear state of the NLP to the quasi-linear state of the DS. The DS state sustains from the 13 572nd to 13 644th RTs and the intensity of the DS was suddenly enhanced at the 13 644th RT. Before collapsing, the DS has strong peak power in the temporal domain; the spectrum of the DS is broadened and then destroyed to the NLP due to the DS collapsing and over-driving of the NPR. The entire dynamics of the transient coherence recovery in Figure 3d are presented in Visualization S2 in Supporting Information. The pulse states in Figure 3c at the 13 490th, 13 538th, 13 645th, and 13 670th RTs are marked with A–D, respectively. We can see from Figure 3e that the single-shot spectra of A and D are the NLP, while B and C are the DS with steep edges. The step edges of the spectra of B and C are caused by the strong chirp of the DS while the oscillating structures at the edges of C are caused by the self-phase modulation-induced nonlinear chirp with strong peak power. Similar to the case in Figure 2e, the pulse in Figure 3e has maximum intensity when it is the coherent DS at C, while it has maximum pulse energy when it is the incoherent NLP at D. The corresponding filed autocorrelation traces (FACs) of Figure 3d are shown in Figure 3f. We can see stochastic structures in pedestals of FAC are suppressed while the width of the central peak increased after the pulse transformed into the coherent DS. As the energy of the DS increases, oscillating structures appear on both sides of the FAC, which demonstrates the strong nonlinear chirp of the DS at the energy peak. After the widespread oscillating structures evolved into the stochastic structures while the central peak narrows, the NLP came into being. The FAC evolution demonstrates that the enhanced nonlinearity drives the DS into the incoherent NLP.

The transient coherence recovery in the present paper is opposite to the soliton explosion process, where the pulse coherence is destroyed and the energy increased.<sup>[13–16]</sup> The process of the soliton explosion can be regarded as the transient coherence loss. We can explain the transient coherence recovery in this paper from the characteristics of the NLP and NPR. The NPR is an artificial SA based on the nonlinear coupling between the orthogonal polarized components of the wave in the laser. When the wave is stochastic such as the NLP, the parameters of the artificial SA fluctuate accordingly. Under a certain state of the SA, as well as the saturated gain of the EDF due to the strong pulse energy, the positive feedback of the SA can be obtain and thus the incoherent NLP recovers to the coherent DS state. After the DS formation, the DS will be strongly amplified due to the recovered gain of the EDF, experiencing strong nonlinear phase accumulation and shifting the NPR to the negative feedback region again. The NLP is generated under the composite effect of the DS wave-breaking and the negative feedback of NPR. In a word, the stochastic feedback on the artificial SA by the NLP plays a key role in the randomly transient coherence recovery.

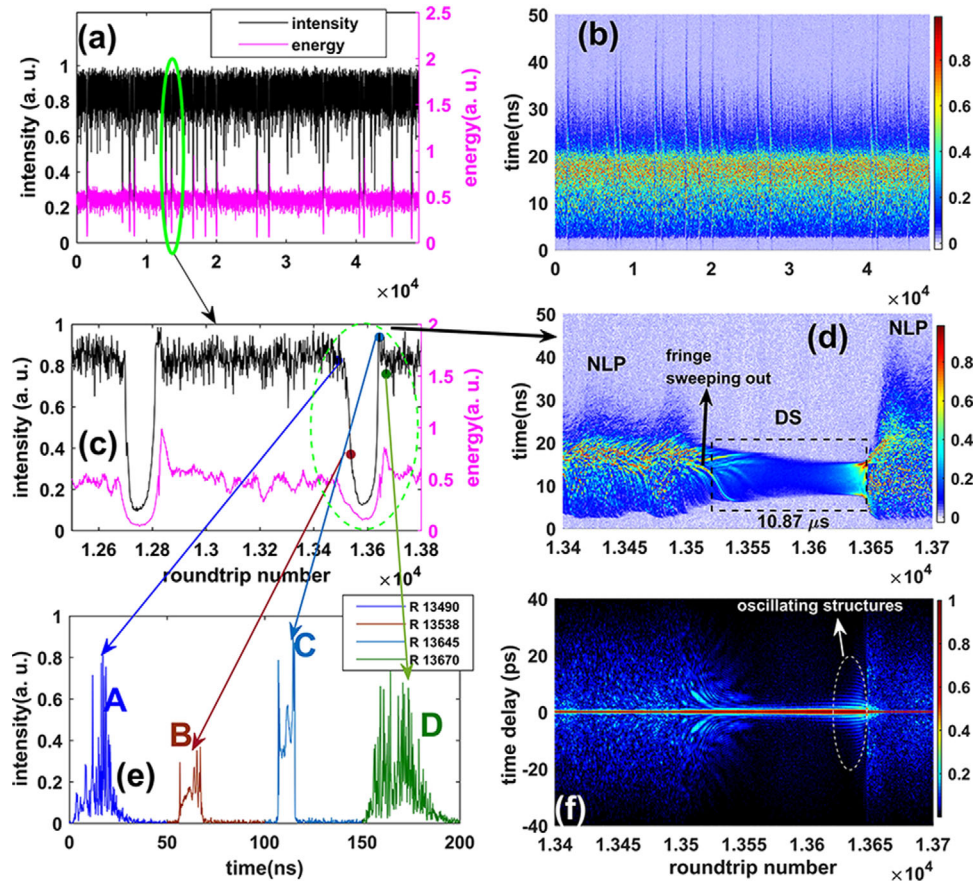


**Figure 3.** Evolution of the stretched signals during the incoherent NLP state in the captured 49 000 RTs. The sampling rate of the OSC is  $40 \text{ GS s}^{-1}$ . a) Intensity and energy evolution of the DFT signal for 49 000 RTs. b) Spatio-spectral evolution of the DFT signals. c) Local enlargement of the marked portion in (a). d) Spatio-spectral evolution of the marked portion in (c). This is the dynamics of the transient coherence recovery embedded in the evolution of the NLP. e) Four single-shot spectra at the 13 490th, 13 538th, 13 645th, and 13 670th RTs. f) The FAC evolution corresponding to the spectra in (d).

#### 2.4. From NLP to Quasi-CW

Another important process in Figure 1 is P1 and the process of the NLP-to-quasi-CW is captured in Figure 4. The NLP transforms into the quasi-CW with the RO as a transition in Figure 4a. There is an additional pulse build-up during the RO as can be seen from the spatio-spectral evolution in Figure 4b. The additional pulse is a new-born pulse from the background. We exclude the possibility of the saturation of the photodetector (PD) for the generation of the additional pulse because the additional pulse still existed when the main pulse is weak from the 25 000th to 30 000th RTs. Figure 4c is the local enlargement of the transition of the NLP to the RO in Figure 4b. The main and additional pulses emerge synchronously at the 12 289th RT after the transient coherence recovery, coexisting with the NLP and Q-switched CW components. After the transient coherence recovery at the 12 289th RT, there are four kinds of wave components in the cavity: the main pulse, additional pulse, Q-switched CW, and NLP. The NLP and Q-switched CW components totally attenuate after the 13 276th and 20 000th RTs, respectively. After the RO, the main pulse gradually decays while the additional pulse increases and then decays to the quasi-CW. The complex NLP-to-quasi-CW process in Fig-

ure 4c is visualized in Visualization S3, Supporting Information. The single-shot spectra of A–D in Figure 4c are shown in Figure 4e. B has the typical spectrum of the DS. From A to C, the pulse experiences the transient coherence recovery. The coexistence of the new-born main pulse, additional pulse, and NLP can all be seen in the spectrum of C. The DFT signal of D has obvious Q-switched CW background as well as the additional pulse.

The RO process in Figure 4 results from the complicate effect of the slow gain dynamics. In addition, there are complicate interactions among the main pulse, additional pulse, CW component, and NLP. After the transient coherence recovery, the parameters of the SA, together with the total laser parameters, make the lasing state transform toward the quasi-CW state while the slow gain dynamics induces the RO process. During the increased RO in Figure 4d, the NLP experiences the saturated gain and the new pulses emerges. The main and additional pulses quickly suppress the NLP through cross-gain-modulation and some other complex process such as the spectral filtering induced multi-pulsing. The main and additional pulses cannot sustain for a long time due to the unbalance gain and loss, gradually transforming into the quasi-CW. Similar results of the decreased RO in ref. [35] show that, by changing the loss of the SA artificially, the ultrafast laser transforms from the mode-locking

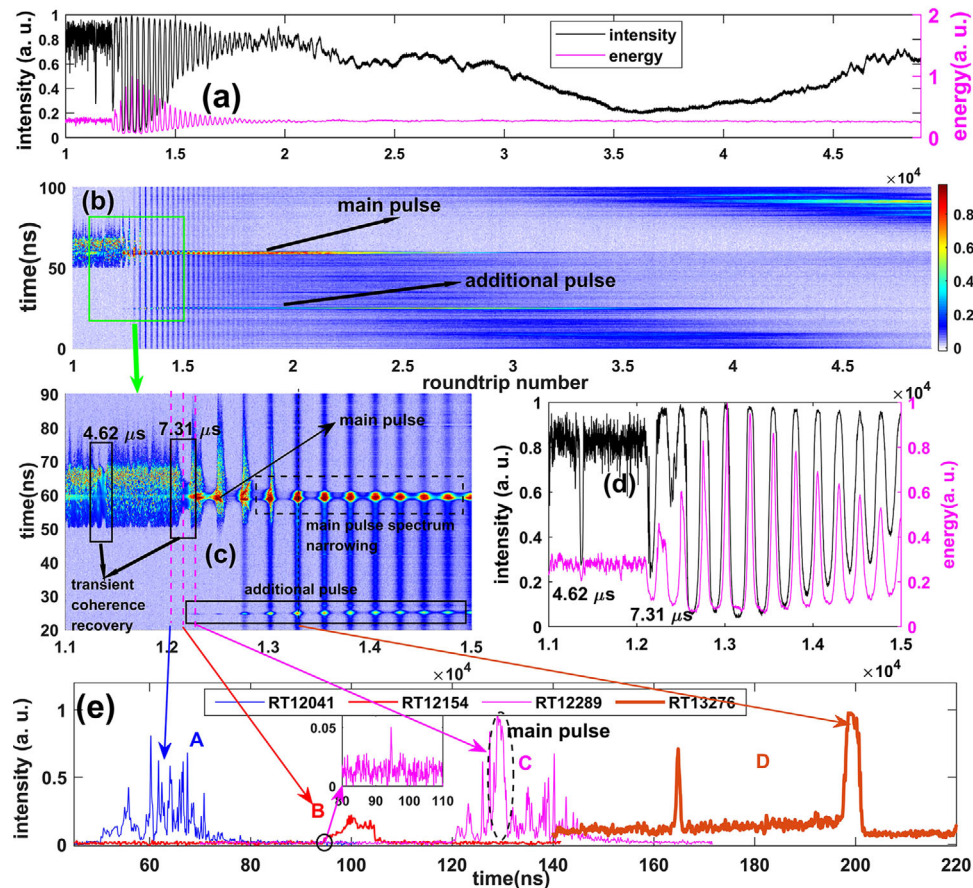


**Figure 4.** Transformation from the NLP to the quasi-CW state in the captured 49 000 RTs. The sampling rate of the OSC is  $40 \text{ GS s}^{-1}$ . a) Intensity and energy evolution of the stretched signal for 49 000 RTs. b) Spatio-spectral evolution of the stretched signals. c) Local enlargement of the marked portion in (b). d) Spatio-spectral evolution of the marked portion in (c). e) Four single-shot spectra at the 12 041st, 12 154th, 12 289th, and 13 276th RTs. The inset in (e) is the local enlargement of the additional pulse of the point C.

to CW or reversely with the Q-switching as a transition. This is almost the same case in our paper, except that the adjustment of SA is caused by the feedback of the pulse on the NPR without external adjustment. By tuning the PC to make the laser work at another state of the composite mode-locking, we have checked that there is always the transient coherence recovery before the RO and a new-born main pulse always emerges after the transient coherence recovery. Our results confirm that the transient coherence recovery is the trigger of the transformation from the NLP into the quasi-CW.

## 2.5. Temporal Dynamics without Time-Stretching

With the laser setting kept fixed, the laser output without the DFT is measured. The input power on the PD is carefully attenuated to avoid saturation as much as possible. Consecutive two CML processes in 190 000 RTs with a sampling rate of  $20 \text{ GS s}^{-1}$  and the results are shown in Figure 5. The interval between two CML is 122 164 RTs or 12.4 ms. Both CML processes in Figure 5a annihilate into the quasi-CW with the decreased RO as the transition. The quasi-CW sustains from the 38 000th to the 110 000th RTs. Figure 5b is the corresponding spatio-temporal evolution of Figure 5a, where we can see a long-term

fluctuation during the quasi-CW state. The local enlargements of the lasing state transitions marked in Figure 5b are shown in Figure 5c–f, respectively. There is a transient power enhancement as marked in Figure 5c,e. Although not the same process, we can see from Figure 2 that there was a transient coherence recovery when the pulse transformed from the quasi-CW into the NLP. In the temporal domain, this means there was a transient peak power enhancement when the pulse becomes a DS during the transient coherence recovery. Thus, the results in Figure 5c,e are in good agreement with the results in Figure 2. The insets in Figure 5e are the single-shot temporal profiles of the pulse at the 131 131st, 131 513rd, and 132 052nd RTs, respectively. The intensity of the NLP state at the 132 052nd RT is weaker than that of the DS state at the 131 513rd RT. The pulse before mode-locking at the 131 131st RT is wide while the component at its heading edge is attenuated after the mode-locking. Similar peak power enhancement also happens during the transformation from the NLP to quasi-CW in Figure 5d, which corresponds to the transient coherence recovery during. A main pulse and the CW background during the decreased RO coexist in Figure 5f, which agrees with the evolution of the time-stretched signal in Figure 4c, except that there is no additional pulse in Figure 5f. The results in Figure 5c–f demonstrate that the peak power of the DS in the transient coherence recovery is actually much stronger

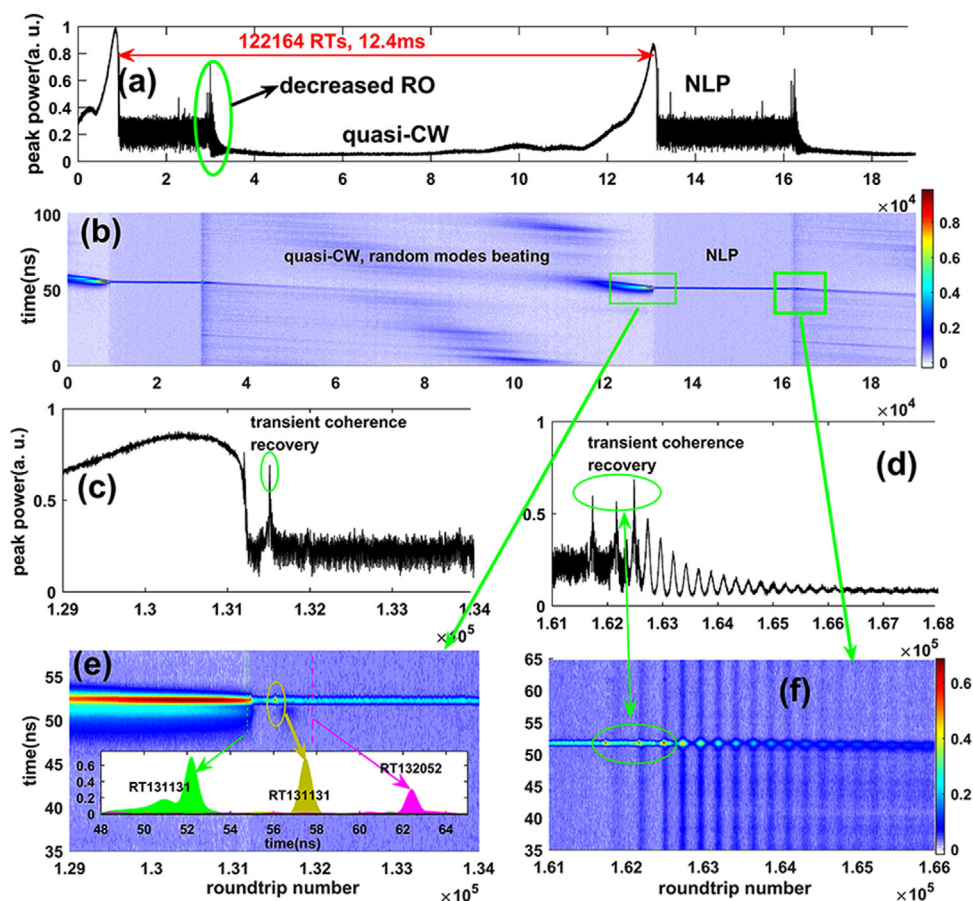


**Figure 5.** Temporal evolution for the captured 190 000 RTs measured without time-stretching. The sampling rate of the OSC is  $20 \text{ GS}^{-1}$ . a) Peak power and energy evolution of the signal. b) Spatio-temporal evolution of the signals. c) Peak power evolution from the 129 000th to 134 000th RTs. d) Peak power evolution from the 129 000th to 134 000th RTs. e) Spatio-temporal evolution corresponding to (c). f) Spatio-temporal corresponding to (d). The insets in (e) are the single-shot intensity profiles of the three marked positions in (e).

than that of the incoherent NLP in temporal domains, which can trigger the subsequent DS collapse and the over-driving of the NPR. Although the temporal measurement is not accurate due to the limited resolution of the PD and OSC, the temporal evolution measured in Figure 5 agrees well with the time-stretched results, which confirms the universal characteristics such as the transient coherence recovery in the lasing state transformations and the RO during the pulse annihilation.

### 3. Discussion

In the fiber lasers mode-locked by the nonlinear amplifier loop mirror or NPR,<sup>[29]</sup> the artificial (based on physical effects rather than on the material properties) SA imposed on the pulse is sensitive to the pulse parameters and evolution dynamics, such as the polarization evolution and nonlinear phase accumulation. The feedback of the pulse on the artificial SA offers the internal perturbation on the pulse in the dissipative systems. Different lasing states coexist but cannot sustain for a long period because of the sustained perturbation induced by the incoherent pulse evolution, resulting in the composite mode-locked state in this paper. The transformation from the NLP to the quasi-CW

is always accompanied by the transient coherent recovery in the experiment, during which the artificial SA is transiently altered to drive the lasing state transformation. Due to the slow dynamics of the EDF, the light experiences RO when the laser transforms from the NLP to the quasi-CW and similar RO processes during the light transition have been researched in different optical systems with EDF.<sup>[37,38]</sup> In this laser, the NLP and quasi-CW can be regarded as dynamic regimes nearby two saddle-focus points connected through heteroclinic-orbits in the phase space of the nonlinear dissipative system while their switching dynamics reminds Shilnikov-type heteroclinic dynamics.<sup>[39]</sup> Similar dynamics was demonstrated in the vector soliton fiber lasers with complex switching between orthogonal states of polarization.<sup>[18,40]</sup> Detailed analysis in terms of the fractal dimension of the experimental and theoretical data series revealed an emergence of a new type of chaotic attractor for some range of the laser parameters.<sup>[18]</sup>

External perturbations have important effects on the build-up and evolution of the mode-locked fiber lasers.<sup>[7,8,20]</sup> In our experimental setup, the stable DS operation can be obtained by only tuning the PC,<sup>[10]</sup> which means the external perturbations are weak. External perturbations on the laser cavity originate from the fluctuations of the pump source and birefringence induced by environmental perturbations. Numerical simulations show that

the DS and NLP can retain their characteristics with even 10% fluctuations of the pump of the EDF, as shown in Figures S3–S5, Supporting Information. Although our simulation results also show that the DS and NLP are sensitive to the fluctuation of the birefringence, the birefringence fluctuation only result in the dramatic evolution, but not the relatively robust lasing state transformation in experiments. Furthermore, the laser system in our experiment is built on a vibration-isolated optical table, so the instant tapping or vibration on the system is minimized. Based on the results of the simulation and experiment, we think the lasing state transformation in our paper is induced by the intrinsic wave evolution dynamics, but not external environment perturbations.

Another CML state through PC tuning is also observed in Figure S2, Supporting Information. The universal characteristics are that the quasi-CW transformed into the NLP without the RO while the NLP-to-quasi-CW is always accompanied with the RO as the transition. This is because when the positive feedback of the artificial SA is destroyed by the transient coherence recovery, the slow-gain dynamics, such as the gain depletion and recovery, dominate the process of the NLP-to-quasi-CW. For the opposite case, the quasi-CW can transform into the NLP without the increased RO when the artificial SA has positive feedback on the pulse. The positive feedback here refers to the global ability of the SA to ensure the localized structure formation, which is slightly different from the term of the positive feedback region of the non-monotonic SA.<sup>[11, 22–24]</sup> We would like to stress that the simulations in Supporting Information are not able to adequately describe the full-dynamics in the experiments with large time scales. This defines an interesting challenge for laser modeling community: to develop an effective simulation method that can accurately describe the coexisting slow dynamics of the CW and fast dynamics and interactions of pulses.

## 4. Conclusion

This study experimentally revealed the dynamics of the spontaneous alternation of mode synchronization and mode desynchronization in a NPR mode-locked fiber laser. The observed dynamics considered in the Poincaré mapping can be regarded as the chaotic attractor for the nonlinear system, where dynamics nearby two saddle-focus points is switched between each other through the heteroclinic-orbits in the phase space. The existence of the transient coherence recovery acts as the trigger for the transitions between two lasing regimes. The transient coherence recovery is also observed during the NLP evolution. We anticipate that the experimentally observed the Shilnikov-type ultrafast dynamics in the form of randomly switching between NLP and quasi-CW regimes is important both for the basic science of distributed dynamical systems corresponding to the optical implementation of the Poincaré mapping and for potential practical applications ranging from secure communications to laser processing of materials. Combining methods of the dynamical systems and ultrafast fiber laser science one can explore rich dynamics of nonlinear dissipative systems. Though complex irregular dynamics in fiber lasers are more difficult to comprehend compared to traditional mode-locking mastering of these high-entropy states might pave a way to new applications of lasers.

## 5. Experimental Section

The laser and measurement setups are shown in Figure S1, Supporting Information. The laser had a total length of 20.7 m, with a net-dispersion of  $\approx 0.754$  ps<sup>2</sup>. The resolution of the DFT measurement was  $\approx 0.138$  nm. We kept the driving current of the LD fixed while adjusting the artificial SA and birefringence through tuning the PC.

## Supporting Information

Supporting Information is available from the Wiley Online Library or from the author.

## Acknowledgements

The authors acknowledge support from National Natural Science Foundation of China (NSFC) (61775074), National Key R&D Program of China (2018YFE0117400), and H2020 MSCA RISE project HALT. The work of S.K.T. was supported by the Russian Science Foundation (Grant No. 17-72-30006).

## Conflict of Interest

The authors declare no conflict of interest.

## Keywords

fiber laser, nonlinear optics, optical spectroscopy

Received: June 30, 2019  
Revised: December 17, 2019  
Published online: February 11, 2020

- [1] M. E. Fermann, I. Hartl, *Nat. Photonics* **2013**, *7*, 868.
- [2] C. Xu, F. W. Wise, *Nat. Photonics* **2013**, *7*, 875.
- [3] K. Goda, B. Jalali, *Nat. Photonics* **2013**, *7*, 102.
- [4] P. Grelu, N. Akhmediev, *Nat. Photonics* **2012**, *6*, 84.
- [5] T. J. Kippenberg, A. L. Gaeta, M. Lipson, M. L. Gorodetsky, *Science* **2018**, *361*, eaan8083.
- [6] N. Akhmediev, J. M. Soto-Crespo, G. Town, *Phys. Rev. E* **2001**, *63*, 056602.
- [7] L. M. Zhao, D. Y. Tang, H. Zhang, X. Wu, *Opt. Express* **2009**, *17*, 8103.
- [8] S. Chouli, P. Grelu, *Phys. Rev. A* **2010**, *81*, 063829.
- [9] K. Sulimany, O. Lib, G. Masri, A. Klein, M. Fridman, P. Grelu, O. Gat, H. Steinberg, *Phys. Rev. Lett.* **2018**, *121*, 133902.
- [10] A. F. J. Runge, C. Agueraray, N. G. R. Broderick, M. Erkintalo, *Opt. Lett.* **2013**, *38*, 4327.
- [11] D. Y. Tang, L. M. Zhao, B. Zhao, *Opt. Express* **2005**, *13*, 2289.
- [12] M. Horowitz, Y. Barad, Y. Silberberg, *Opt. Lett.* **1997**, *22*, 799.
- [13] S. T. Cundiff, J. M. Soto-Crespo, N. Akhmediev, *Phys. Rev. Lett.* **2002**, *88*, 073903.
- [14] M. Liu, A. P. Luo, W. C. Xu, Z. C. Luo, *Opt. Lett.* **2016**, *41*, 3912.
- [15] Y. Q. Du, X. W. Shu, *Opt. Express* **2018**, *26*, 5564.
- [16] A. F. J. Runge, N. G. R. Broderick, M. Erkintalo, *Optica* **2015**, *2*, 36.
- [17] J. M. T. Thompson, H. B. Stewart, *Nonlinear Dynamics and Chaos*, 2nd ed., Wiley, New York **2002**.
- [18] S. V. Sergeev, C. B. Mou, E. G. Turitsyna, A. Rozhin, S. K. Turitsyn, K. Blow, *Light: Sci. Appl.* **2014**, *3*, e131.

- [19] Y. Q. Du, X. W. Shu, *Opt. Express* **2017**, *25*, 28035.
- [20] L. M. Zhao, D. Y. Tang, H. Zhang, X. Wu, *Opt. Express* **2008**, *16*, 10053.
- [21] Y. Q. Du, X. W. Shu, *IEEE Photonics J.* **2018**, *10*, 150911.
- [22] Z. C. Cheng, H. H. Li, P. Wang, *Opt. Express* **2015**, *23*, 5972.
- [23] D. J. Li, D. Y. Tang, L. M. Zhao, D. Y. Shen, *J. Lightwave Technol.* **2015**, *33*, 3781.
- [24] Y. J. Lyu, X. H. Zou, H. X. Shi, C. Liu, C. Wei, J. F. Li, H. P. Li, Y. Liu, *Opt. Express* **2017**, *25*, 13286.
- [25] A. Komarov, H. Leblod, F. Sanchez, *Phys. Rev. A* **2005**, *71*, 053809.
- [26] M. Anderson, Y. D. Wang, F. Leo, S. Coen, M. Erkintalo, S. G. Murdoch, *Phys. Rev. X* **2017**, *7*, 031031.
- [27] F. Leo, L. Gelens, P. Emplit, M. Haelterman, S. Coen, *Opt. Express* **2013**, *21*, 9180.
- [28] C. Y. Bao, W. K. Chang, C. X. Yang, N. Akhmediev, S. T. Cundiff, *Phys. Rev. Lett.* **2015**, *115*, 253903.
- [29] H. A. Haus, E. P. Ippen, K. Tamura, *IEEE J. Quantum Electron.* **1994**, *30*, 200.
- [30] E. P. Ippen, *Appl. Phys. B: Lasers Opt.* **1994**, *58*, 159.
- [31] A. Mahjoubfar, D. V. Churkin, S. Barland, N. Broderick, S. K. Turitsyn, B. Jalali, *Nat. Photonics* **2017**, *11*, 341.
- [32] G. Herink, B. Jalali, C. Ropers, D. R. Solli, *Nat. Photonics* **2016**, *10*, 321.
- [33] X. M. Liu, X. K. Yao, Y. D. Cui, *Phys. Rev. Lett.* **2018**, *121*, 023905.
- [34] P. Ryczkowski, M. Narhi, C. Billet, J. M. Merolla, G. Genty, J. M. Dudley, *Nat. Photonics* **2018**, *12*, 221.
- [35] Z. C. Luo, J. Q. Kang, M. Liu, C. Li, C. H. Kong, Y. Yu, K. K. Y. Wong, *IEEE Photonics Technol. Lett.* **2018**, *30*, 1803.
- [36] Y. Q. Du, Z. W. Xu, X. W. Shu, *Opt. Lett.* **2018**, *43*, 3602.
- [37] G. Okhotnikov, J. R. Salcedo, *Opt. Lett.* **1994**, *19*, 1445.
- [38] D. Abraham, R. Nagar, V. Mikhelashvili, G. Eisenstein, *Appl. Phys. Lett.* **1993**, *63*, 2857.
- [39] C. P. Silva, *IEEE Trans. Circuits Syst. I* **1993**, *40*, 675.
- [40] H. Khashi, S. V. Sergeyev, C. B. Mou, A. M. Garcia, M. A. Araimi, A. Rozhin, S. Kolpakov, V. Kalashnikov, *Ann. Phys. (Berlin)* **2018**, *530*, 1700362.